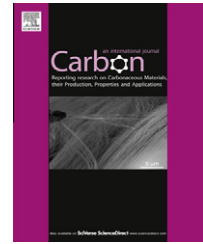


Available at www.sciencedirect.com

SciVerse ScienceDirect

journal homepage: www.elsevier.com/locate/carbon

In situ synthesis of metal oxides in carbon nanotube arrays and mechanical properties of the resulting structures

Jordan R. Raney^a, Hong-Li Zhang^b, Daniel E. Morse^b, Chiara Daraio^{a,*}

^a Division of Engineering and Applied Science, California Institute of Technology, 1200 E. California Blvd., MC 105-50, Pasadena, CA 91125, USA

^b Institute for Collaborative Biotechnologies and Center for Energy Efficient Materials, University of California, Santa Barbara, CA 93106-5100, USA

ARTICLE INFO

Article history:

Received 9 January 2012

Accepted 4 May 2012

Available online 18 May 2012

ABSTRACT

In the past, aligned arrays of carbon nanotubes (CNTs) have been observed to exhibit a foam-like dissipative response in compression, garnering attention for possible mechanical applications. Nanoparticles have previously been integrated with graphitic materials for electrochemical applications. Here, we synthesize nanoparticles of SnO₂ and MnO₂ in the interstices of aligned arrays of CNTs without altering the ordered structure of the arrays, and we characterize their mechanical response. We report that CNT arrays with embedded particles present superior energy dissipation relative to unmodified CNT arrays. In addition, energy dissipation, strain recovery, and structural failure (observed after repeated loading) depend on particle type (SnO₂ versus MnO₂).

© 2012 Elsevier Ltd. All rights reserved.

1. Introduction

The remarkable mechanical properties of carbon nanotubes (CNTs) have received much attention [1], leading to many efforts to design materials that realize macroscale advantages through integrating these nanoscale structures [2]. Among the approaches taken, it has been noted that nominally aligned arrays (or “forests”) of millimeter-scale CNTs can be readily synthesized via standard chemical vapor deposition (CVD) techniques. These materials exhibit behavior similar to fatigue-resistant, open-cellular foams under compression [3,4], with significant recovery from deformation and orders of magnitude superior energy dissipation relative to commercial foams of comparable density (0.1–0.3 g cm⁻³) [5].

Recent attempts have been made to understand structure–property relationships for these materials, such as how the bulk mechanical response is affected by various structural features [6–8]. In these studies, synthesis parameters were altered to obtain CNT arrays with different features, allowing the study of how CNT surface roughness [6], CNT diameter

distribution [7], or partially-graphitic layering around individual CNTs [8] affects the bulk mechanical response. The control of these synthesis parameters, combined with the modification of CNT arrays after synthesis (such as by the infiltration of polymer into array interstices [9] or by the incorporation of surfactants and nanoparticles via solvent wetting [10]), allows for tuning of the mechanical response, such as array stiffness and energy dissipation, under compression.

Here we develop a novel approach for modifying the mechanical response of CNT arrays post-synthesis. Namely, we reinforce the CNT arrays by coating the individual CNT surfaces or filling the interstices of the arrays with metal oxide particles. We adopt two different procedures to synthesize MnO₂ and SnO₂ particles in the CNT arrays. For the synthesis of MnO₂ particles, we use a solution-based approach, as described in more detail later. For the synthesis of SnO₂ particles, we use a kinetically-controlled catalytic synthesis approach, similar to that used in the past for growing Sn particles *in situ* in graphitic anodes for electrochemical applications [11]. In both cases, the particles are synthesized *in situ*

* Corresponding author.

E-mail address: daraio@caltech.edu (C. Daraio).

0008-6223/\$ - see front matter © 2012 Elsevier Ltd. All rights reserved.

<http://dx.doi.org/10.1016/j.carbon.2012.05.021>

in the CNT arrays. In contrast, most work in the past involving nanoparticle modification of CNTs has been performed on disordered arrangements of CNTs that have first been dispersed in solution (often an acid) and then filtered. Such procedures have been performed to synthesize particles on disordered arrangements of CNTs such as ZnO [12], Au [13], Ni [14], CaCO₃ [15], Cu [16], and others [17]. Specifically relevant to this work, SnO₂ nanoparticles have been integrated with disordered arrangements of CNTs in the past using CVD [18] and solution-based techniques [19]. MnO₂ particles have also been integrated with disordered CNTs [20,21]. Such materials have already been created in the past for various electrochemical applications, such as aqueous supercapacitors [22]. Thus, these materials based on disordered agglomerates of surface-modified CNTs are useful for certain applications, and do not require the infiltration of particles deep inside CNT arrays, which can be a challenge for many synthesis approaches. While dispersing the CNTs into disordered arrangements prior to modification avoids the problem of needing to obtain good particle infiltration into the arrays, it necessitates the loss of the ordered structure of CNT arrays. For most applications, such a CNT powder must be integrated into another, usually polymeric, matrix. This process has many challenges of its own, such as the difficulty in obtaining uniform dispersion of the CNTs in the matrix [23].

Here, we seek to improve the mechanical performance of CNT arrays without disrupting their ordered structure. We investigate the mechanical stability of these hybrid CNT–nanoparticle structures, which could be useful in multifunctional applications. Inorganic materials have been infiltrated into ordered CNT arrays previously. A sol–gel process has been used to create a CNT–glass composite, but the focus was on enhancing thermal and electrical conductivities of the materials [24]. Low pressure CVD has also been used, but only for very short CNT arrays (~50 μm) due to difficulties in getting reactions to take place more than a few tens of microns deep in the array [25]. More recently a vapor-assisted technique has been used to successfully synthesize TiO₂ uniformly in short CNT arrays, a procedure possibly generalizable to other types of oxides in the future [26]. However, none of these studies examined how the presence of the nanoparticles affects the mechanical properties of CNT arrays, which is important for understanding issues such as mechanical stability. Here we obtain dispersion of particles deep within millimeter-scale arrays without altering the crystalline structure of the individual CNTs or the ordered arrangement of them. In addition to modifying the CNT arrays we test them under quasistatic compression to examine how energy dissipation, strain recovery, loading/unloading modulus, and permanent damage are affected by the modifications. Understanding these mechanical properties is also a necessary first step toward the use of materials based on nanoparticle–CNT array structures in relevant applications, such as electrochemical applications that have recently been investigated [27].

2. Experimental

We synthesized arrays of multiwall carbon nanotubes (CNTs) using a thermal chemical vapor deposition (CVD) system and

a floating catalyst approach described in the past [7,28]. Our growth substrate was thermally oxidized Si placed in a CVD furnace set to 827 °C. We injected a 0.02 g ml⁻¹ solution of ferrocene (a precursor of Fe, a catalyst for CNT synthesis) and toluene (a carbon source for CNT synthesis) at a rate of 1 ml min⁻¹ using a syringe pump into the heating zone, with Ar as a carrier gas. This approach results in continued deposition of new catalyst, and thereby continued initiation of new CNT growth, throughout the synthesis process. CNT array samples (with typical heights of 1–1.5 mm, areal cross sections of 10–20 mm², volume occupied by CNTs ~10%, and individual CNT diameters of 40–50 nm, as characterized by transmission electron microscopy in our previous work [7]) were removed from their growth substrates using a razor blade. The mass for each of these samples was measured using a microbalance, and this was used to calculate the bulk density, both before and after synthesis of the oxide particles.

Loading of SnO₂ particles followed steps similar to those discussed in previous work [11]. CNT samples were first added to aqueous SnCl₂ (0.2 M, 5 ml), with 0.6 ml of acetone added to aid absorption into the array. After soaking for 46 h at room temperature, the CNT samples were fully wetted with the SnCl₂ solution and placed in a sealed container that contained an open solution of ammonia (2 wt.%). The ammonia vapor gradually diffused to the sample, initiating hydrolysis of the SnCl₂ solution contained inside the CNT array. The samples were then removed and washed with deionized water, followed by further heat treatment in N₂ at 450 °C for 1 h at the heating rate of 5 °C min⁻¹, yielding the final CNT/SnO₂. To load MnO₂ particles into the CNT arrays, we soaked the CNT samples in aqueous KMnO₄ (0.2 M, 5 ml) for 46–120 h (with the variation in time controlling the loading amount) at room temperature. During the soaking, MnO₄⁻ spontaneously reduced to MnO₂ on the surface of the CNTs, which acted as a reducing agent [21]. After soaking, the sample was subjected to further heat treatment in N₂ at 450 °C for 1 h at a heating rate of 5 °C min⁻¹, yielding the final CNT/MnO₂. Whether modifying the CNT arrays with SnO₂ or MnO₂, there was no observable change in the dimensions of CNT arrays (as can sometimes be observed due to solvent wetting effects). Scanning electron microscopy (SEM) was used to obtain images of sample structure at different magnifications and locations for each sample. By counting the number of CNTs crossing an arbitrary horizontal line at different locations it was determined that there were no statistically significant changes in the spacing of individual CNTs.

Two samples with SnO₂ and five samples with MnO₂ were synthesized following the procedures above, and compared to the performance of three unmodified control samples. Samples were repeatedly compressed quasistatically, using a commercial materials test system (Instron E3000), to 0.8 strain (with strain being defined as the displacement normalized by sample height; i.e., 0.8 strain is equivalent to compressing the sample until it is only 20% of its original height). This compression occurred at a strain rate of 0.03 s⁻¹ (i.e., 3% of the original sample height every second). For each modified CNT array an unmodified “control” sample was tested that had been removed from the growth substrate directly adjacent to it, and therefore had almost the exact same height, density, mean CNT diameter, etc., prior to modification.

Energy dissipation per unit volume was obtained by integrating the area of the stress–strain hysteresis for each loading cycle. The loading modulus was calculated by examining the initial slope of the stress–strain curve. The unloading modulus was similarly calculated by taking the slope of the stress–strain curve after unloading from maximum strain had just begun (specifically, the slope is obtained from the line that connects the point at maximum stress and strain to the point at which the stress upon unloading has dropped to 2/3 of the maximum stress).

Thermogravimetric analysis (TGA, Mettler–Toledo 851e instrument) was conducted at 550 °C in air to quantify the amount (wt.%) of particle loading for each modified sample. The type of oxide was determined after synthesis of the particles using X-ray diffraction (XRD, Philips X'PERT MPD with Cu K α radiation). Samples were characterized with scanning electron microscopy using a FEI Quanta 200F, and transmission electron microscopy using a FEI TF30UT at 300 kV.

3. Results and discussion

After synthesizing oxide nanoparticles in the CNT arrays with various loadings (i.e., different quantities of SnO₂ or MnO₂ as quantified by wt.%) following the procedures described in

Section 2, samples were characterized with scanning electron microscopy (SEM) and transmission electron microscopy (TEM). Fig. 1 compares SEM images of an unmodified array (Fig. 1a) with one modified with SnO₂ (Fig. 1b) and two instances of arrays modified with MnO₂ (Fig. 1c and d). These images illustrate that the way in which the nanoparticles modify the CNT arrays depends strongly on particle type (i.e., SnO₂ versus MnO₂). In all cases, the images are representative of the appearance at this scale at every location internal to the arrays at which it was investigated (i.e., there is no apparent formation of separate densified or cell regions, as determined by SEM images at many different locations and magnifications). The SnO₂ particles formed conglomerations in the array interstices, forming pockets of oxide rather than coating the individual CNTs (Fig. 1b). The MnO₂ particles, in contrast, formed uniformly along the individual CNTs (Fig. 1c and d). This is in agreement with earlier qualitative observations that MnO₂ forms a more uniform, tightly-bound coating around CNTs than SnO₂ [22]. We expect that the different affinities are a result of the different roles that the CNTs play in the two different reactions. As described in Section 2, the synthesis of SnO₂ is performed from aqueous SnCl₂ precursor contained in the CNT array, using a hydrolyzing agent (ammonia) to cause the precipitation of Sn(OH)Cl that

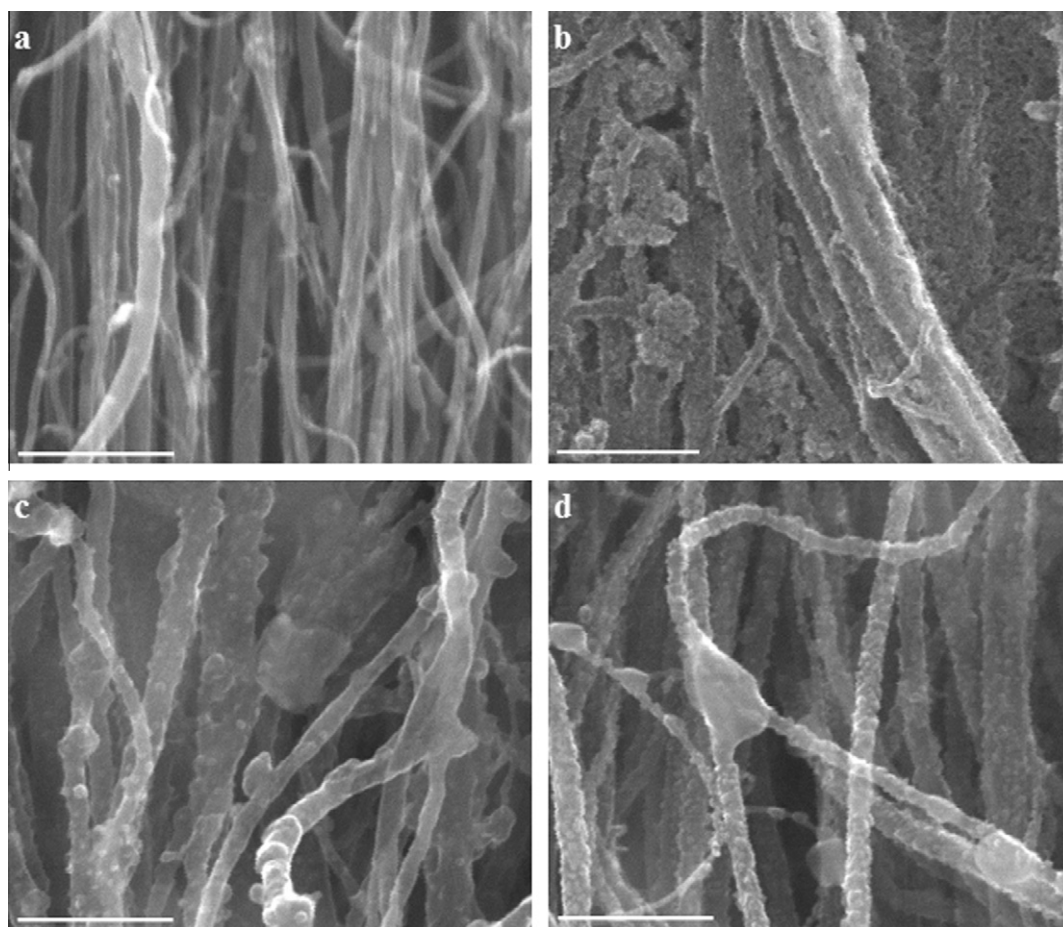


Fig. 1 – Different types of CNT modifications (scale bars are 400 nm); (a) unmodified CNTs; (b) CNT array modified with SnO₂, which has conglomerated in the array interstices and (c and d) two different MnO₂ loadings, both of which predominantly coated the individual CNTs themselves rather than forming conglomerations in the interstices.

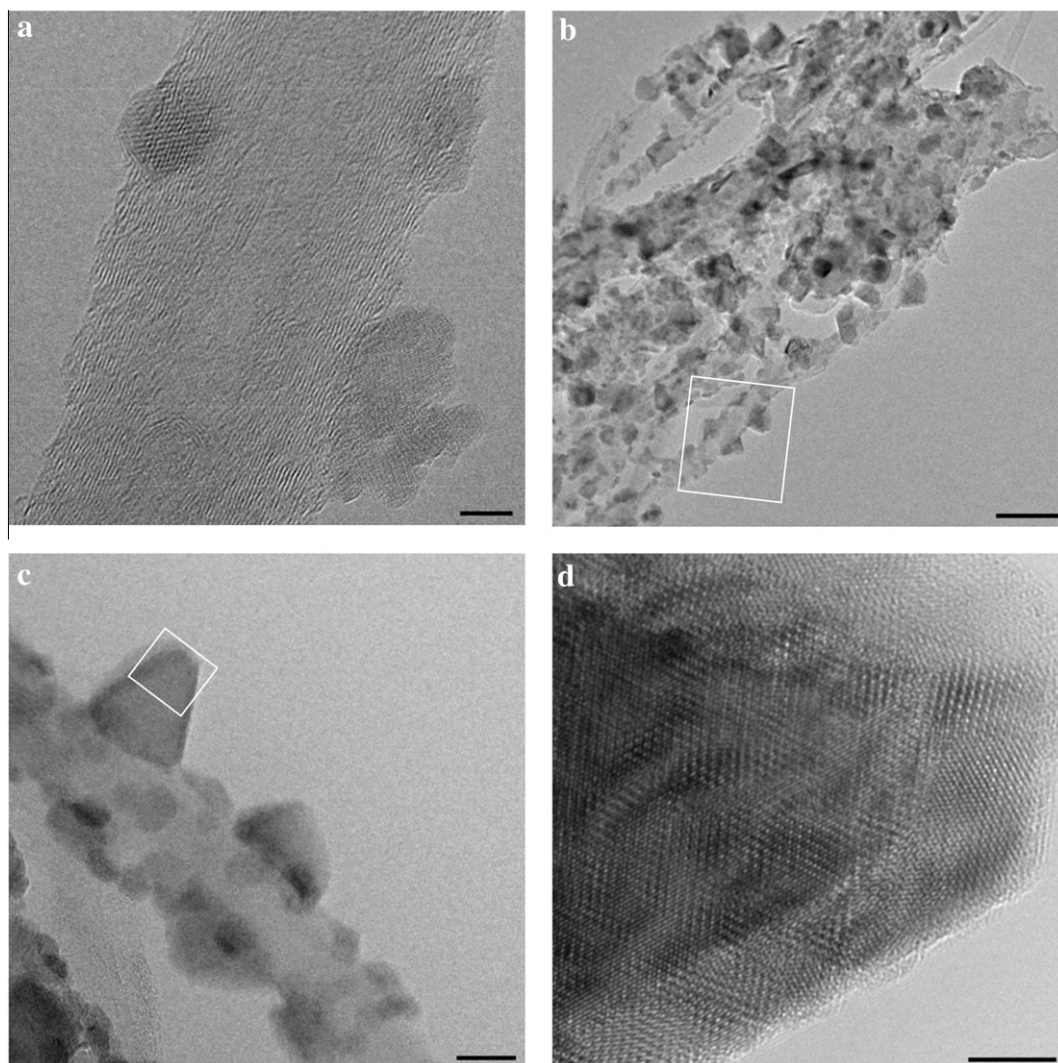


Fig. 2 – Transmission electron microscope images of CNTs modified with MnO₂; (a) high resolution image showing individual CNT walls and crystalline MnO₂ particles (scale bar is 5 nm); (b) a group of aligned CNTs modified with MnO₂ particles (scale bar is 100 nm); (c) a closer view of a single CNT corresponding to the white box in panel b (scale bar is 20 nm) and (d) a high resolution image of a MnO₂ particle corresponding to the white box in panel c (scale bar is 5 nm).

is converted to SnO₂ in the subsequent heat treatment. In this case, the CNT array just provides a substrate/space to accommodate the SnO₂ but does not play an active role in the reaction. For the synthesis of MnO₂, with aqueous KMnO₄ as precursor, the CNTs can take a more active role in the reaction, acting as both a reducing agent and a substrate for MnO₂ precipitation [20,21]. This results in particles being formed mainly on CNTs, not everywhere in the interstices. Two different examples are given for MnO₂ (Fig. 1c and d) in which the particle synthesis parameters used were nearly the same yet slightly different morphological features developed. The sample in Fig. 1c has a lower total amount of MnO₂ loaded relative to the sample in Fig. 1d due to a shorter soak time in the KMnO₄ precursor solution, despite having significantly larger particles. Past observations have shown that the morphology of nanoparticles resulting from the MnO₂ synthesis is highly sensitive to local pH and temperature [21]. Minor variations in these parameters could there-

fore explain the observed morphological differences. As small as these morphological differences are, they may affect mechanical properties, as discussed later.

TEM images for CNT samples modified with MnO₂ are given in Fig. 2. High resolution images reveal the individual walls of the CNTs and the crystalline nature of the attached MnO₂ particles (Fig. 2a). Approximately a dozen roughly aligned CNTs with many MnO₂ particles are shown entangled together (Fig. 2b), displaying a similar morphology to that shown in earlier SEM images (i.e., Fig. 1c). Higher magnification images show the interface between a CNT and particles (Fig. 2c) and a high resolution view of one of these particles (Fig. 2d). The strong interaction between MnO₂ particles and CNTs observed in these images is not seen in the case of SnO₂ particles. It should be noted, however, that, despite the affinity of the MnO₂ particles for the CNTs, TEM did not reveal any damage to the CNT walls or partial embedding of the particles into the walls.

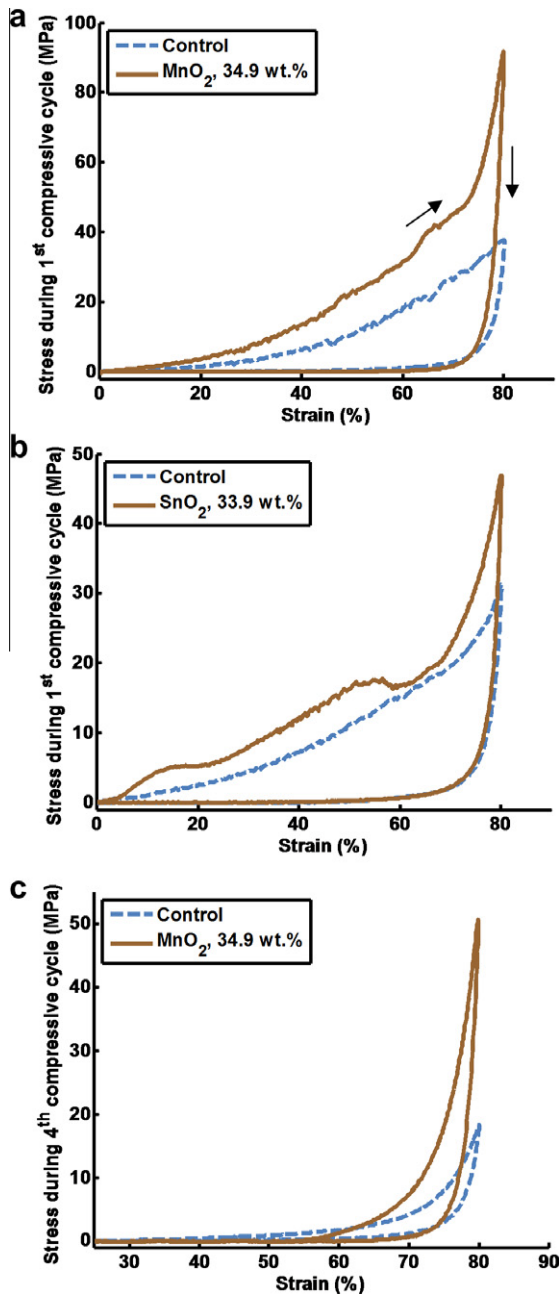


Fig. 3 – Stress–strain relationship of modified CNT arrays relative to their unmodified counterparts; (a and b) the MnO_2 modified samples display a larger improvement in energy dissipation (area of the hysteresis) relative to their control samples than do the SnO_2 modified samples relative to their control samples and (c) by the 4th compressive cycle the samples in panel a both dissipate less energy than in earlier cycles, but the sample reinforced by MnO_2 still has a larger hysteresis than the unmodified sample.

Representative compressive stress–strain responses for samples modified with MnO_2 and SnO_2 are given in Fig. 3a and b, respectively, with the response of corresponding control samples indicated by the dashed lines. A hysteretic response was observed in all cases, as is typical for CNT arrays under compression to large strains [4], with separate

loading and unloading paths (following the path indicated by the arrows in Fig. 3a). Similar stress–strain curves were gathered for numerous samples, and were used to calculate loading modulus (slope of the initial linear region corresponding to small strains), unloading modulus (the slope of the curve at high strain, right after the peak value has been reached and unloading has begun), and energy dissipation. These quantities are summarized in Table 1. The area of the stress–strain hysteresis represents the energy dissipated per unit volume. Note the greater improvement in energy dissipation for the sample modified with MnO_2 relative to its control (Fig. 3a), approximately 100% improvement in this case, as compared to the sample modified with SnO_2 relative to its control (Fig. 3b), about 42% improvement in this case. Superior energy dissipation was consistently observed for samples loaded with MnO_2 relative to those loaded with SnO_2 .

In addition to these differences resulting from the different particle types, there may be an effect from particle morphology even within a given category of particle type. As mentioned earlier, the slight morphological differences between the samples displayed in Fig. 1c and d (both modified with MnO_2) could contribute to the differences in energy dissipation between the two cases, with the former dissipating approximately 70% more energy than the latter during equivalent compression tests. This is noteworthy particularly because the latter sample, with less energy dissipation, was actually loaded with a higher quantity of MnO_2 (40.2 wt.% rather than 34.9 wt.%).

We examined how the samples responded under repeated compressive loading. One of the intriguing properties of as-grown CNT arrays synthesized by floating catalyst CVD is their ability to dissipate energy and to recover much of their original height even after many compressive cycles to high strain (0.8 or higher) [3,4]. The first cycle generally reaches the highest peak stress and dissipates the largest quantity of energy, with a significant drop in these for the second cycle. After only a few compressive cycles, however, the material begins to reach a steady state response that does not vary significantly from cycle to cycle [7]. In this study we observed that the response to repeated loading depended strongly on whether the sample was reinforced with MnO_2 or instead with SnO_2 . Samples modified with MnO_2 are observed to have higher peak stress and larger hysteresis area (i.e., energy dissipation) than their respective control samples even for repeated compressive cycles (Fig. 3c). The same is not observed for samples modified with SnO_2 , which by the fourth cycle show a nearly identical mechanical response to their respective control samples.

Fig. 4 illustrates in more detail the significant difference between the response of samples modified with MnO_2 under repeated loading and that of the samples modified with SnO_2 . Because the unmodified control samples also show decreased performance with repeated loading, Fig. 4 shows the responses of modified samples relative to this changing response of the control samples (i.e., the first compressive cycle for the modified samples are compared to the first cycle of the unmodified samples, the second compressive cycle for the modified samples to the second cycle of the unmodified samples, etc.). Fig. 4a shows relative energy dissipation for the first four compressive cycles. As already discussed, the

Table 1 – Loading and unloading modulus and energy dissipation per unit volume of modified and unmodified samples.

| | Loading mod., cyc 1 (MPa) | Loading mod., cyc 4 (MPa) | Unloading mod., cyc 1 (MPa) | Unloading mod., cyc 4 (MPa) | En. dissipation, cyc 1 (MJ m^{-3}) | En. dissipation, cyc 4 (MJ m^{-3}) |
|----------------|------------------------------|------------------------------|--------------------------------|--------------------------------|--|--|
| Control | 6.6 ± 3.8 | 3.1 ± 1.8 | 1710 ± 330 | 900 ± 290 | 6.89 ± 0.49 | 0.71 ± 0.18 |
| SnO_2 | 41 ± 8 | 2.4 ± 0.6 | 2860 ± 230 | 1090 ± 150 | 9.71 ± 0.58 | 0.60 ± 0.05 |
| MnO_2 | 9.3 ± 5.6 | 23 ± 6 | 4170 ± 400 | 3180 ± 190 | 13.0 ± 1.6 | 1.40 ± 0.24 |

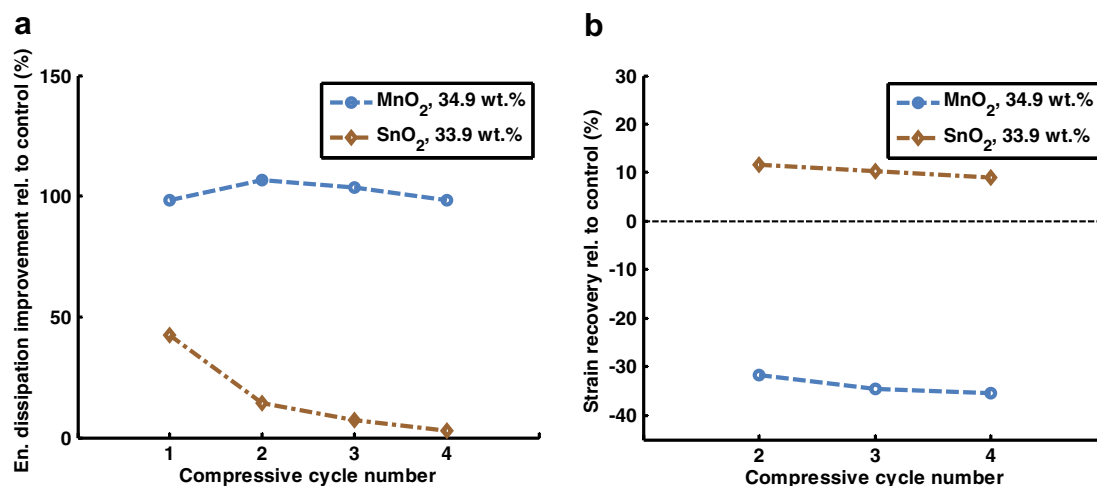


Fig. 4 – Mechanical performance of modified CNT arrays relative to their unmodified counterparts for repeated loading; (a) both MnO_2 and SnO_2 modified samples dissipate more energy during compression than control samples, but the performance improvement for samples with SnO_2 is almost entirely gone by the fourth compressive cycle; (b) though samples with MnO_2 dissipate more energy than both SnO_2 and control samples, they do not recover strain as well after compression.

sample modified with MnO_2 dissipated approximately 100% more energy than did its control during the first compressive cycle. It continued to dissipate approximately 100% more energy than the control sample in subsequent cycles as well. In the case of samples modified with SnO_2 , however, by the fourth compressive cycle the material behaved almost identically to the control, dissipating approximately the same amount of energy and attaining approximately the same peak stress (Fig. 4a).

In terms of energy dissipation for repeated loading, it is clear that the properties of CNT arrays modified with MnO_2 particles are superior to those modified with SnO_2 , which lose all advantages over their control within a few compressive cycles. However, when strain recovery is considered the samples respond in the opposite manner. Fig. 4b shows the initial heights of the modified samples relative to those of their respective control samples at the beginning of each compressive cycle. This indicates the amount of strain that the CNT array recovers after the previous compressive cycle. With the control samples indicated by the horizontal line at 0% (by definition), it is clear that samples modified with MnO_2 recovered significantly less strain after compression than did either the control samples or those modified with SnO_2 . The latter actually recovered slightly more strain after compression than the control samples, which may be related to disruption of some of the lateral entanglement between CNT bundles.

It is also useful to examine the loading and unloading moduli to better understand the compressive response under repeated loading cycles. As summarized in Table 1, the initial loading moduli for samples modified with SnO_2 have an average value (41 ± 8 MPa) approximately an order of magnitude higher than those of either the unmodified samples or those modified with MnO_2 . However, by the fourth cycle (see Table 1) the average loading modulus for samples with SnO_2 has dropped by an order of magnitude to closely match the average value for unmodified samples. In contrast, samples with MnO_2 show a substantial increase in loading modulus after a few cycles. All samples show a dramatic decrease in unloading modulus after the first cycle, though the samples with MnO_2 show a decrease of a smaller relative value.

The results discussed above and displayed in Fig. 4 can be explained by returning to the SEM images in Fig. 1 to understand the different morphologies that result from modifying the CNTs by either SnO_2 or MnO_2 . As discussed, the SnO_2 particles appear to form interstitial conglomerations without substantially modifying the individual CNTs (Fig. 1b) whereas the MnO_2 particles form directly on the individual CNT surfaces (Fig. 1c and d). It is useful to combine these observations with top down SEM images taken of the samples after they were repeatedly compressed, which indicate how the materials tend to fail (Fig. 5). Note that the samples modified with SnO_2 display many lateral cracks that form perpendicular to the long CNT axes (Fig. 5a). Such behavior is in accordance

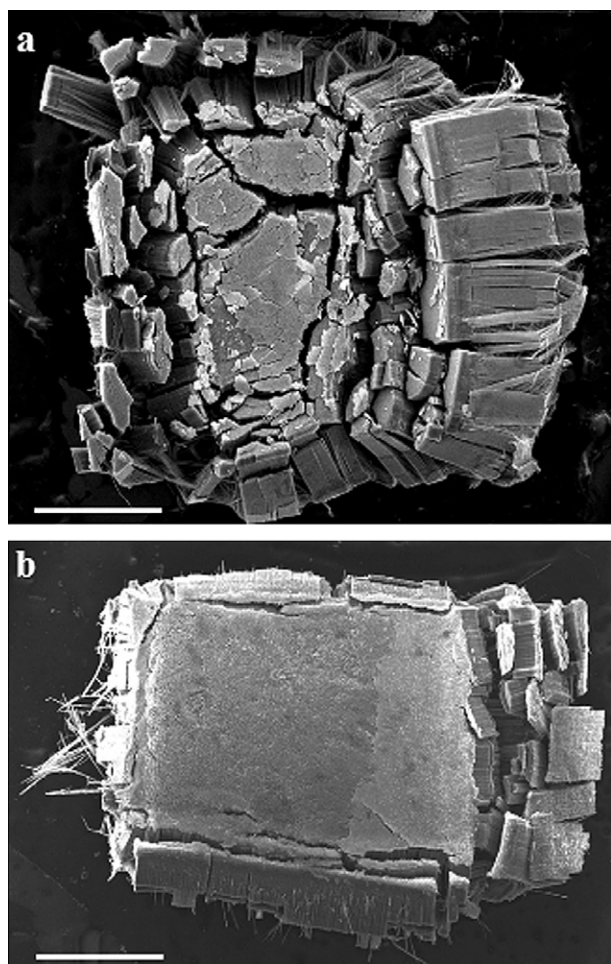


Fig. 5 – Top down scanning electron microscope images for the assessment of material failure after several compressive cycles to 0.8 strain (scale bars are 1 mm); (a) CNT array modified with SnO₂, exhibiting many lateral cracks and (b) CNT array modified with MnO₂ displaying much less lateral cracking comparatively.

with the morphology displayed in Fig. 1b, in which brittle pockets of oxide between elastic CNT bundles would serve as natural locations of fracture. This also explains the high loading modulus obtained in the first cycle, with a large contribution from the oxide deposits, followed by very low values of loading modulus for later cycles, since the oxide deposits would have already failed in brittle fashion (Table 1). With these parallel brittle and elastic elements in compression the material fractures into small elastic bundles of CNTs. After the first couple of cycles these elastic bundles no longer interact as strongly with one another, causing the loss of the initial improvement in energy dissipation with repeated loading (Fig. 4a). Concomitantly, once the oxide is fractured and no longer coupling adjacent CNT bundles, the recovery of the material after compression will be entirely driven by the elastic CNTs, which are known to be highly resilient against bending and buckling [29,30], not inhibited by the fractured oxide deposits. This results in the large strain recovery for

samples modified by SnO₂ shown in Fig. 4b. In marked contrast, the samples modified with MnO₂ show very little lateral cracking (Fig. 5b), in accordance with a morphology predominantly consisting of individually modified CNT surfaces (Fig. 1c and d) rather than large deposits of oxides between separated CNT bundles. With this morphology it would be expected that the mechanical response would be driven by interactions between individual CNTs rather than the material breaking into separated CNT bundles. The result is consistently improved energy dissipation even after repeated compressive loading (Fig. 4a) but poor strain recovery due to significant entanglement among the individual CNTs in the compressed state (Fig. 4b). This is also in agreement with the increase in loading modulus for the samples modified with MnO₂ (Table 1). Because samples modified with MnO₂ do not recover well from compression, they remain in a densified state. This increased density for later compressive cycles corresponds to an increased loading modulus.

Fig. 6 illustrates this discussion in the form of diagrams and additional SEM images for clarity. Fig. 6a represents a sample modified with SnO₂ that is compressed, requiring the brittle fracture of oxide between CNT bundles, followed by recovery driven by the now uninhibited elastic CNT bundles. Fig. 6b and c provide a view from the side and top of the CNT array, respectively, using SEM. Notice that the side view shows excellent recovery of the CNT bundles, and the top view shows significant separation of the bundles. In contrast, the samples modified with MnO₂ (Fig. 6d–f) show little cracking but recover much less of their original height after compression. Fig. 6e and f show significant permanent entanglement of individual CNTs at two different magnifications.

This discussion also explains the existence of plateaus in the stress–strain curves for samples modified with SnO₂ (e.g., Fig. 3b) which are not observed for the samples modified with MnO₂ (e.g., Fig. 3a). It is noteworthy that such plateaus are only observed for the first compressive cycle, and are therefore thought to correspond to brittle failure during the formation of lateral cracks through the oxide deposits. It is clear from Fig. 5b that even the samples modified by MnO₂ display some lateral cracking along the edges of the samples after compressive loading. This can occur to some extent even in unmodified CNT arrays due to a lack of inward lateral support at the edges.

In addition to Sn and Mn oxides we also synthesized Fe oxide and Co oxide particles using corresponding metal salts as precursors and following similar procedures as described earlier. We have also successfully formed metallic particles by subjecting the oxide particles to carbothermal reduction. While we have thereby verified the versatility of the processes described in this study as a proof of concept, further work is necessary, including the synthesis of a larger number of such samples, to understand the systematic effects of these different types of particle loadings on the mechanical properties. It is especially important to understand the integrity of these structures under mechanical stresses by understanding how the affinities of the various types of particles for CNTs might differ from one another, as we have done for SnO₂ and MnO₂.

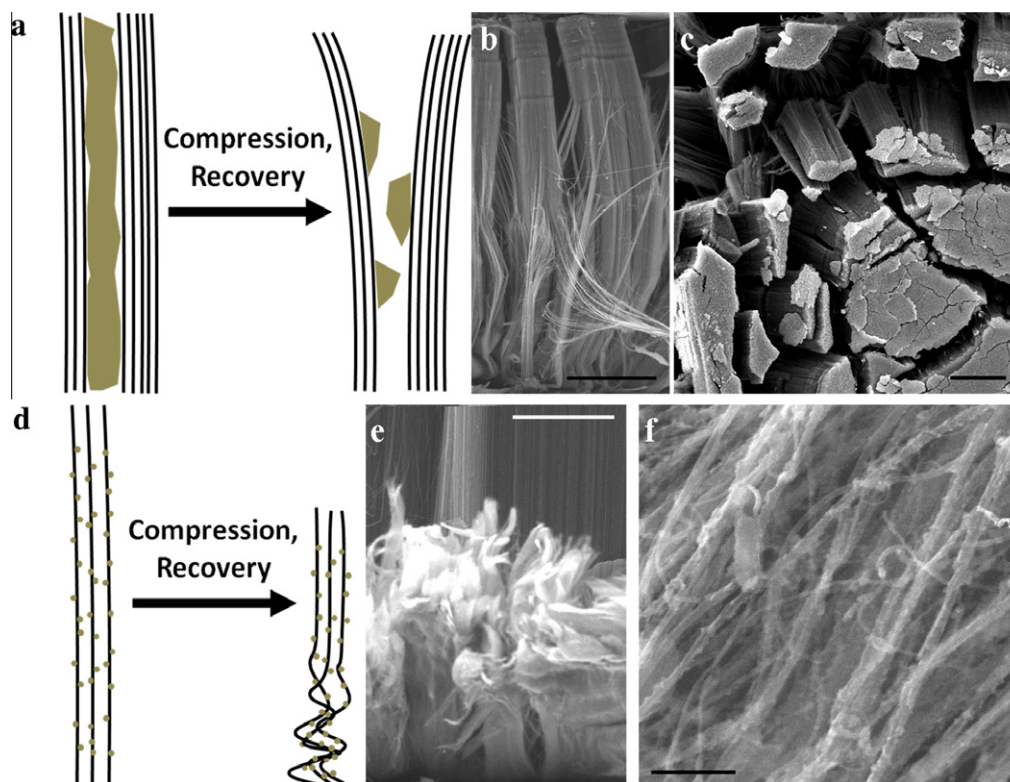


Fig. 6 – CNT morphology before and after compression and recovery for samples modified with SnO₂ (panels a–c) and MnO₂ (panels d, e and f); (a) SnO₂ forms in clumps between CNT bundles, leading to brittle fracture and lateral cracking during compression followed by CNT-driven partial elastic recovery; (b and c) SEM images of the SnO₂-modified CNT array after compression and recovery from both the side and top, respectively (scale bars are 250 μm); (d) MnO₂ forms as smaller particles along each CNT, leading to entanglement after compression, and less subsequent strain recovery; (e) SEM image taken from the side of a MnO₂-modified CNT array near the base, where compressive deformation predominates (scale bar is 100 μm) and (f) an image from the same region as in panel e but at higher magnification (scale bar is 500 nm).

4. Summary

We have synthesized SnO₂ and MnO₂ in CNT arrays without disrupting the ordered structure of the individual CNTs or the overall structure of the arrays themselves. Under compression the structures exhibit a hysteretic response, as expected for CNT arrays. The structures modified with nanoparticles dissipate up to twice the amount of energy as unmodified samples. Modifying CNT arrays with SnO₂ results in brittle deposits of the oxide in the array interstices separated by elastic bundles of CNTs. Compressing these structures results in lateral fracturing through the oxide deposits, followed by elastic recovery of the CNT bundles. After only a few compressive cycles the material with SnO₂ responds similarly to unmodified CNT arrays in compression (as compared by quasistatic stress–strain data). In contrast to this, when MnO₂ particles are synthesized in CNT arrays by immersion of the CNTs in aqueous KMnO₄ the particles form on the individual CNTs themselves. The modifications result in higher energy dissipation during compression and minimal lateral fracturing, even after repeated cycling, but also yield more entanglement of the individual CNTs, resulting in less strain recovery after compression. With electrochemical applications already being developed for similar materials, continued

study of the mechanical properties of these systems could lead to useful multifunctional materials with simultaneous mechanical and electrochemical uses.

Acknowledgements

The authors thank Carol Garland for her assistance with transmission electron microscopy. This work is supported by the Institute for Collaborative Biotechnologies, under contract W911NF-09-D-0001 with the Army Research Office. JRR also gratefully acknowledges support from the Department of Defense via a National Defense Science and Engineering Graduate (NDSEG) fellowship.

REFERENCES

- [1] Qian D, Wagner GJ, Liu WK, Yu M, Ruoff RS. Mechanics of carbon nanotubes. *Appl. Mech. Rev.* 2002;55(6):495–532.
- [2] Liu L, Ma W, Zhang Z. Macroscopic carbon nanotube assemblies: preparation, properties, and potential applications. *Small* 2011;7(11):1504–20.

- [3] Suhr J, Victor P, Ci L, Sreekala S, Zhang X, Nalamasu O, et al. Fatigue resistance of aligned carbon nanotube arrays under cyclic compression. *Nat. Nanotechnol.* 2007;2(7):417–21.
- [4] Cao AY, Dickrell PL, Sawyer WG, Ghasemi-Nejhad MN, Ajayan PM. Super-compressible foamlike carbon nanotube films. *Science* 2005;310(5752):1307–10.
- [5] Misra A, Raney JR, De Nardo L, Craig AE, Daraio C. Synthesis and characterization of carbon nanotube multilayer structures. *ACS Nano* 2011;5(10):7713–21.
- [6] Bradford PD, Wang X, Zhao H, Zhu YT. Tuning the compressive mechanical properties of carbon nanotube foam. *Carbon* 2011;49(8):2834–41.
- [7] Raney JR, Misra A, Daraio C. Tailoring the microstructure and mechanical properties of arrays of aligned multiwall carbon nanotubes by utilizing different hydrogen concentrations during synthesis. *Carbon* 2011;49(11):3631–8.
- [8] Li X, Ci L, Kar S, Soldano C, Kilpatrick SJ, Ajayan PM. Densified aligned carbon nanotube films via vapor phase infiltration of carbon. *Carbon* 2007;45(4):847–51.
- [9] Ci L, Suhr J, Pushparaj V, Zhang X, Ajayan PM. Continuous carbon nanotube reinforced composites. *Nano Lett.* 2008;8(9):2762–6.
- [10] Misra A, Raney JR, Craig AE, Daraio C. Effect of density variation and non-covalent functionalization on the compressive behavior of aligned carbon nanotubes. *Nanotechnology* 2011;22:425705.
- [11] Zhang HL, Morse DE. Kinetically controlled catalytic synthesis of highly dispersed metal-in-carbon composite and its electrochemical behavior. *J. Mater. Chem.* 2009;19(47):9006–11.
- [12] Guo G, Guo J, Tao D, Choy WCH, Zhao L, Qian W, et al. A simple method to prepare multi-walled carbon nanotube/ZnO nanoparticle composites. *Appl. Phys. A.* 2007;89(2):525–8.
- [13] Moon SY, Kusunose T, Tanaka S, Sekino T. Easy synthesis of a nanostructured hybrid array consisting of gold nanoparticles and carbon nanotubes. *Carbon* 2009;47(12):2924–32.
- [14] Bittencourt C, Felten A, Ghijsen J, Pireaux JJ, Drube W, Erni R, et al. Decorating carbon nanotubes with nickel nanoparticles. *Chem. Phys. Lett.* 2007;436(4–6):368–72.
- [15] Liu Y, Wang R, Chen W, Chen X, Hu Z, Cheng X, et al. Kabob-like carbon nanotube hybrids. *Chem. Lett.* 2006;35(2):200–1.
- [16] Zhao B, Yadian BL, Li ZJ, Liu P, Zhang YF. Improvement on wettability between carbon nanotubes and Sn. *Surf. Eng.* 2009;25(1):31–5.
- [17] Eder D. Carbon nanotube – inorganic hybrids. *Chem. Rev.* 2010;110(3):1348–85.
- [18] Kuang Q, Li SF, Xie ZX, Lin SC, Zhang XH, Xie SY, et al. Controllable fabrication of SnO₂-coated multiwalled carbon nanotubes by chemical vapor deposition. *Carbon* 2006;44(7):1166–72.
- [19] Han WQ, Zettl A. Coating single-walled carbon nanotubes with tin oxide. *Nano Lett.* 2003;3(5):681–3.
- [20] Jin X, Zhou W, Zhang S, Chen GZ. Nanoscale microelectrochemical cells on carbon nanotubes. *Small* 2007;3(9):1513–7.
- [21] Ma SB, Ahn KY, Lee ES, Oh KH, Kim KB. Synthesis and characterization of manganese dioxide spontaneously coated on carbon nanotubes. *Carbon* 2007;45(2):375–82.
- [22] Ng KC, Zhang S, Peng C, Chen GZ. Individual and bipolarly stacked asymmetrical aqueous supercapacitors of CNTs/SnO₂ and CNTs/MnO₂ nanocomposites. *J. Electrochem. Soc.* 2009;116:A846–53.
- [23] Xie XL, Mai YW, Zhou XP. Dispersion and alignment of carbon nanotubes in polymer matrix: a review. *Mater. Sci. Eng., R* 2005;49(4):89–112.
- [24] Otieno G, Koos AA, Dillon F, Wallwork A, Grobert N, Todd RI. Processing and properties of aligned multi-walled carbon nanotube/aluminoborosilicate glass composites made by sol-gel processing. *Carbon* 2010;48(8):2212–7.
- [25] Chandrashekar A, Ramachandran S, Pollack G, Lee JS, Lee GS, Overzet L. Forming carbon nanotube composites by directly coating forests with inorganic materials using low pressure chemical vapor deposition. *Thin Solid Films* 2008;517(2):525–30.
- [26] Neocleus S, Pattinson SW, Moissala Motta AM, Windle AH, Eder D. Hierarchical carbon nanotube-inorganic hybrid structures involving CNT arrays and CNT fibers. *Func. Mater. Lett.* 2011;4(1):83–9.
- [27] Wang W, Epur R, Kumta PN. Vertically aligned silicon/carbon nanotube (VASCNT) arrays: hierarchical anodes for lithium-ion battery. *Electrochem. Commun.* 2011;13(5):429–32.
- [28] Andrews R, Jacques D, Rao AM, Derbyshire F, Qian D, Fan X, et al. Continuous production of aligned carbon nanotubes: a step closer to commercial realization. *Chem. Phys. Lett.* 1999;303(5–6):467–74.
- [29] Falvo MR, Clary GJ, Taylor RM, Chi V, Brooks FP, Washburn S, et al. Bending and buckling of carbon nanotubes under large strain. *Nature* 1997;389(6651):582–4.
- [30] Yakobson BI, Brabec CJ, Bernholc J. Nanomechanics of carbon tubes: instabilities beyond linear response. *Phys. Rev. Lett.* 1996;76(14):2511–4.